HHS Public Access

Author manuscript

ACS Nano. Author manuscript; available in PMC 2023 October 25.

Published in final edited form as:

ACS Nano. 2022 October 25; 16(10): 16211–16220. doi:10.1021/acsnano.2c05098.

Autonomous untethered microinjectors for gastrointestinal delivery of insulin

Arijit Ghosh[1,#], **Wangqu Liu**[1,#], **Ling Li**[2], **Gayatri J. Pahapale**[1], **Si Young Choi**[1], **Liyi Xu**[1], **Qi Huang**[1], **Ruili Zhang**[1], **Zijian Zhong**[1], **Florin M. Selaru**[2,3,*], **David H. Gracias**[1,3,4,5,6,7,8,*]

[1]Chemical and Biomolecular Engineering, Johns Hopkins University, Baltimore, MD 21218, USA

[2]Gastroenterology and Hepatology, Department of Medicine, Johns Hopkins University School of Medicine, Baltimore, MD 21287, USA

[3]Sidney Kimmel Comprehensive Cancer Center (SKCCC), Johns Hopkins University School of Medicine, Baltimore, MD 21287, USA

[4]Department of Oncology, Johns Hopkins University School of Medicine, Baltimore, MD 21287, USA

[5]Center for Microphysiological Systems, Johns Hopkins University School of Medicine, Baltimore, MD 21287, USA

[6]Department of Chemistry, Johns Hopkins University, Baltimore, MD 21218, USA

[7]Materials Science and Engineering, Johns Hopkins University, Baltimore, MD 21218, USA

[*]**Corresponding Authors** David H. Gracias; dgracias@jhu.edu; Florin M. Selaru; fse1arul@jhmi.edu.
[#]AG and WL contributed equally to this work.

Author Contributions

AG, DHG, and FMS conceptualized the study and designed the experiments; DHG and FMS supervised the study; AG, WL, LX, SC, and RZ performed the microfabrication and *in vitro* device characterization; GP carried out the gel imaging studies; AG, WL, LL, and LX performed the animal experiments; AG, LX, and QH did the SEM and μ-CT imaging of tissues; AG did the bioanalysis and pharmacokinetic data analysis; WL, LL and ZZ performed the histology study; WL and AG made the illustrations; AG, WL, FMS and DHG wrote the manuscript with input from all authors.

Competing interests: Johns Hopkins University has filed patents related to the technology. Under an option to license agreement between Kley Dom Biomimetics, LLC and the Johns Hopkins University, Prof. D. H. Gracias and the Johns Hopkins University are entitled to royalty distributions related to the technology described in the study discussed in this publication. This arrangement has been reviewed and approved by the Johns Hopkins University in accordance with its conflict-of-interest policies. In addition, some of the authors and the Johns Hopkins University have patents/patent applications related to the technology described.

Supporting Information

Supporting Information is available free of charge at https://pubs.acs.org/doi/

The supporting information contains:

Supporting Notes:

Note S1: Design of the microinjectors; Note S2: Microinjector safety consideration; Note S3: Optimization of the thermoresponsive trigger layer deposition; Note S4: Estimation of the force and pressure exerted by the microinjector tips; Note S5: Validation of the enzyme-linked immunoassay (ELISA) assay; Note S6: Microinjectors insulin delivery efficiency compared with other methods; Note S7: Theoretical estimation of microinjectors' tissue damage.

Supporting Figures:

Figure S1: Schematics showing the design and fabrication of the bidirectional foldable microinjectors; Figure S2: Optimization of the paraffin wax deposition conditions; Figure S3: Microinjectors on tissue-mimicking gelatin; Figure S4: Microinjectors penetrating the pig stomach/colon mucosa.; Figure S5: Additional rat colon histology after microinjector actuation; Figure S6: Microinjector *in vitro* drug release profile; Figure S7: Standard curve showing absorbance vs. insulin concentration at 450 nm; Figure S8: Validation of the non-specificity of the ELISA assay to intrinsic rat insulin.

Supporting Movie:

Movie SM1: Video showing thermo-responsive actuation of bidirectionally folding microinjectors sped up 50 times.

[8]Laboratory for Computational Sensing and Robotics (LCSR), Johns Hopkins University, Baltimore, MD 21218, USA

Abstract

The delivery of macromolecular drugs *via* the gastrointestinal (GI) tract is challenging as these drugs display low stability as well as poor absorption across the intestinal epithelium. While permeation-enhancing drug delivery methods can increase the bioavailability of low molecular weight drugs, the effective delivery of high molecular weight drugs across the tight epithelial cell junctions remains a formidable challenge. Here, we describe autonomous microinjectors that are deployed in the GI tract, then efficiently penetrate the GI mucosa to deliver a macromolecular drug, insulin, to the systemic circulation. We performed *in vitro* studies to characterize insulin release and assess the penetration capability of microinjectors and we measured the *in vivo* release of insulin in live rats. We found that the microinjectors administered within the luminal GI tract could deliver insulin trans-mucosally to the systemic circulation at levels similar to those with intravenously administered insulin. Due to their small size, tunability in sizing and dosing, wafer-scale fabrication, and parallel, autonomous operation, we anticipate that these microinjectors will significantly advance drug delivery across the GI tract mucosa to the systemic circulation in a safe manner.

Graphical Abstract

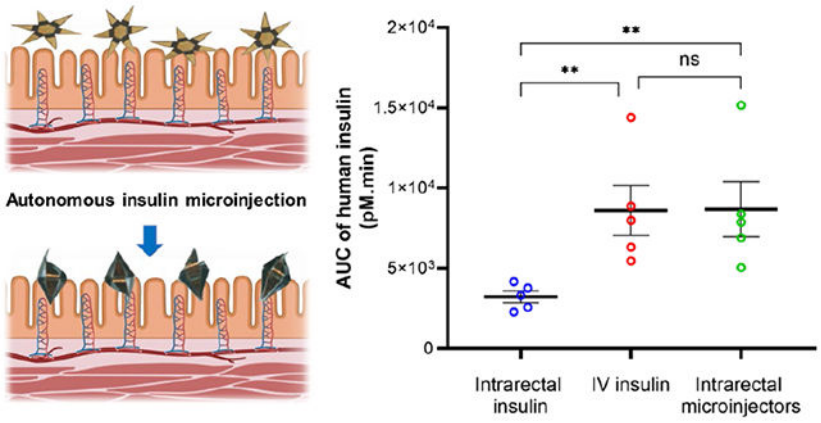

Keywords

robotics; self-folding; drug delivery; oral insulin; shape change

A century ago, Frederick Banting and Charles Best successfully isolated insulin from the dog pancreas and demonstrated that it could reduce blood glucose levels upon injection.[1] Since then, insulin has been the mainstay in managing insulin-dependent diabetes, which currently affects more than 450 million people globally.[2] Insulin is a peptide with a molecular weight of about 5.8 kDa. Like most macromolecular drugs, it is administered by subcutaneous or intravenous (IV) injections. The injection route of insulin delivery poses several limitations, including poor patient compliance and increased risk of infections, thus compromising optimal outcomes. Transdermal and oral insulin delivery routes are

superior in terms of compliance and have been investigated extensively over the past several decades.[3,4] Transdermal insulin delivery systems such as microneedle patches have been explored as alternatives as they are significantly less painful than hypodermic or subcutaneous needles.[5,6] On applying pressure, the microneedles create minuscule disruptions in the stratum corneum, which is the main physical barrier for transporting large molecules like insulin across the skin.[7-10] However, transdermal delivery using microneedle patches has proven challenging due to the difficulty of achieving therapeutic levels of insulin. An alternative to transdermal delivery, the oral administration of insulin has been a long-sought-after goal because of the wide acceptance of the oral route of drug delivery.[11-16] The oral route for insulin delivery has been elusive to date due to several significant hurdles: (i) the degradation of insulin by enzymes like proteases and the acidic pH in the stomach, (ii) the passage of insulin through the mucus barrier that lines the GI epithelium, and (iii) the movement of insulin across the intestinal epithelial cells held together by tight-junction proteins.[17-19] Over the past few decades, the use of permeation enhancers (PE) such as ethylenediaminetetraacetic acid (EDTA), glyceryl monocaprate, and sodium cholate have increased both the paracellular and transcellular transport of insulin in the GI tract[20-22]. However, most PEs are developed based on epithelial monolayer cultures and isolated tissue, which often results in low bioavailability in live animals and therefore has limited potential for clinical translation. [23,24]

An entirely different approach to achieve systemic delivery of insulin from luminal administration is to disrupt the GI epithelial tissue barrier mechanically and physically inject the drug through the epithelium, in the vicinity of blood vessels.[25,26] Several challenges need to be overcome to implement this method, including exerting sufficient force to penetrate epithelium inside the GI tract, unlike transdermal drug delivery, where the patch can be manually pressed against the skin. In recent years, ingestible devices demonstrating this concept include the dynamic omnidirectional adhesive microneedle system (DOAMS), the luminal unfolding microneedle injector (LUMI), the self-orienting millimeter-scale applicator (SOMA), and the RaniPill capsule. These devices exploit the controlled release of energy from steel springs embedded in the device to deliver therapeutics. The relatively large size of the needles and strong forces generated by the spring in these devices pose the risk of perforating the GI tract.[25-28] In addition, these devices have components that are large enough to raise the possibility of GI tract obstruction, particularly in certain pathological conditions which lead to narrowing of the GI tract, such as inflammatory bowel disease, and strictures of a variety of etiologies.[29] These devices are still in the early stage of preclinical/clinical trials, and thus the safety and efficacy of these devices need to be evaluated.

Here, we report the development and operation of robotic, shape-changing microinjectors with an overall size of 1.5 mm when open and around 500 μm when closed, which can autonomously deliver insulin across the GI epithelium. The robotic microinjectors use thermally triggerable energy stored in prestressed thin films, effectively acting as a micro-spring-loaded latches that can release force to enable shape change and facilitate the penetration of the injection tips into the epithelium (Figure 1a). We utilized insulin as a model macromolecular drug and incorporated insulin-loaded chitosan gel patches on the arms of the microinjectors to safely deliver insulin systemically. It is noteworthy that, unlike many larger GI injection devices that are assembled by hand, our microinjectors can be

fabricated using highly parallel wafer-scale processes, like those used in the semiconductor industry, and are scalable across sizes. Moreover, the microinjectors are small enough to be used in large numbers without causing any GI blockage or visible trauma in the animals. Our proof-of-concept studies in rodents show that shape-changing miniaturized injectors administered enterally can safely deliver insulin systemically. Lastly, the bioavailability of insulin delivered *via* the microinjectors is similar to that delivered by an IV injection.

RESULTS AND DISCUSSION

We based the design of the robotic microinjectors on origami principles [30-33] in which each microinjector consists of several hinges and tip segments. The hinge segments of the microinjector generate the injection force necessary for the tips to penetrate the tissue. The injection force is produced by the thermally triggered release of intrinsic differential stress in thin film multilayers of chromium (Cr) and gold (Au) at the hinge.[32-33] Each microinjector is fabricated as a 1.5 mm tip-to-tip 2D multilayer device, which can self-fold to form a 500 μm 3D device. The microinjectors are equipped with six injection arms, 450 μm in length, which are coated with a mucoadhesive chitosan gel loaded with insulin (Figure 1). Notably, we incorporated a bidirectional foldable design of the microinjectors that allows the injection arms to deliver the drug irrespective of the orientation in which they land on the GI epithelium.

Each microinjector is a multilayer thin film structure consisting of five layers (Figure S1a). We used computer-aided drawing (CAD) to design photomasks for patterning individual layers during the fabrication process and can accommodate 483 microinjectors on a 3 in. diameter silicon wafer. This number can be scaled up easily to several thousand per wafer if the fabrication is carried out on a 12 in. diameter wafer, which is routinely used in semiconductor foundries, thus further bringing down the fabrication cost. Figure 1b shows fabricated microinjectors aside rice grains, indicating their small size. We achieved folding bidirectionality of the microinjection arms by engineering the design of the multilayer thin film stacks such that hinges could bend in opposite directions (Figure S1b). We fabricated microinjectors with this design by depositing two different thin film multilayer assemblies: (i) a two-layer assembly of Cr/Au and (ii) a four-layer assembly of Cr/Au/Cr/Au. We estimated the relative thicknesses of the layers in these designs using a theoretical model which optimizes folding angle based on the thicknesses, differential stresses, moduli, and Poisson ratios (details in Note S1). On top of the differentially stressed multilayers, we electrodeposited thick nickel (Ni)/Au rigid panels on the center and tip segments. The microinjector regions with such rigid panels do not bend, whereas the thinner hinges bend and fold autonomously when thermally actuated. We note that all the metallic materials used to fabricate the microinjectors are considered nontoxic in their elemental form, and they have been widely used in biomedical applications (additional details in Note S2).

Moreover, due to the continuous renewal of the GI mucosa, the microinjectors are entirely removed from the GI tract within a few days (additional details in Note S2). We spatially patterned insulin-loaded chitosan gel patches on the microinjector arms using a combination of photolithography and electrodeposition, as described in a previous study (Figure 1c,d).[33] Finally, we patterned a paraffin wax trigger layer atop the hinges of the microinjectors (Note

S3); this layer softens at the physiological temperature of the GI tract and acts as the thermal trigger to induce the bending of the hinges and folding of the microinjectors. A schematic of the entire fabrication process flow is shown in Figure S1c. After fabrication (Figure 1e), we released the microinjectors from the silicon wafer and stored them at room temperature (approximately 23 °C) or in a refrigerator (approximately 4 °C). When administered from the cold state, we observed that the injection arms activate within a few minutes once the microinjectors equilibrate with the physiological temperature of the GI tract (Figure 1f and Movie SM1).

The microinjector arms with insulin-loaded chitosan gel layers were approximately 5 μm in thickness (Figure 2a,b). This thin size and sharp shape of the tip of the microinjector arms are necessary to generate a high pressure to penetrate tissue at the injection site. We theoretically estimated the maximum pressure exerted by the microinjection arm tips to be 0.4-0.5 MPa for the arms with the drug-loaded chitosan layer and 0.5-0.6 MPa for the arms without chitosan gel using the Hertz contact mechanics model (Note S4). Note that although the dimensions and design are different, the pressure exerted by the microinjector arm tips is consistent with previously described theragrippers.[33]

We evaluated the injection performance of the microinjectors on gelatin hydrogels having a stiffness of 1 kPa, which is close to the stiffness of the colonic mucosa (~0.7 kPa) (Figure 2c). [34] The preparation of thermally stable gelatin is described in the Materials and Methods section.[35] For ease of visualization, we used rhodamine dye as a model drug and actuated the microinjectors by placing them in an oven set at 40 °C for 15-20 min (Figure S3) to simulate the physiological temperature. We selected 40 °C for injection performance studies because it allows the microinjectors to actuate faster avoiding the dehydration of samples in the incubator. On actuation, we observed that the microinjector arms penetrated approximately 300 μm into the 1 kPa gel (Figure 2d). We also conducted similar experiments with a significantly stiffer gelatin hydrogel (35 kPa) to estimate the microinjection tip penetration depth in a stiff tissue environment (Figure 2d). We found that the microinjector arms could only penetrate up to 100 μm into the 35 kPa gel, whereas it could penetrate up to 3 times the depth into 1 kPa gelatin biomimetic hydrogel. (Figure 2e).

The performance of the microinjectors was then evaluated *ex vivo* on freshly resected rat colon tissue. We placed the microinjectors on top of the rat colon tissue which was incubated in a Petri dish covered with saline (Figure 3a, b). We heated the tissue and injector assembly in an oven to 40 °C (Figure 3c) and evaluated the tissue penetration abilities of the microinjectors using scanning electron microscopy (SEM) and microcomputed tomography (μ-CT). As shown in Figure 3d-g, the microinjectors penetrated approximately 250 μm into the rat colon mucosa, which is similar to the gel penetration experiment results. We also conducted similar experiments on a freshly excised pig stomach as well as colon, and the results are shown in Figure S4.

We also performed histological studies to demonstrate the penetration of microinjectors on colon tissue and assess the effects of microinjector tip insertion on tissue. It is challenging to obtain images of tissue slices, with a microinjector attached to it, as the very small size of the microinjector tips makes it difficult to section along the desired cross section. Thus, after

the actuation of the microinjectors on freshly excised rat colon tissue, we used a cryostat to prepare the tissue slices by frozen sectioning. We embedded the tissue sample in the optimal cutting temperature compound (OCT) and trimmed the frozen sample along the insertion direction of the microinjector arms until the inserted microinjector was observed (Figure 4a). Then we sectioned the tissue and loaded the tissue slice on glass slides. Figure 4b shows the microscopic image of the tissue section acquired after cutting the tissue sample in Figure 4a. We observed that the microinjector tips penetrated the rat colon tissue and resulted in two incisions in the tissue, at depths of 259 and 332 μm. To visualize the release and diffusion from the microinjectors into the colon tissue, we loaded fluorescent dye Rhodamine 6G into the chitosan patch of microinjector tips. In the microscopic fluorescent image of the tissue slide (Figure 4c), we observed strong fluorescence on the dye-loaded microinjector tip sections. The tissue around the incisions created by the microinjector tip also exhibited fluorescence, indicating the presence of the dye gel patch and diffused dye into the tissues around the insertion sites. Note that, in this experiment, we only let microinjectors set on the tissue for 10–15 min for actuation before we embedded and froze the tissue. At *in vivo* release, we anticipate that the microinjectors will remain inserted for extended periods, allowing greater release and deeper diffusion into the tissue. We conducted hematoxylin and eosin (H&E) staining of the tissue slides to better evaluate the effects of microinjector tip insertion on the colon tissue. The image of the H&E-stained tissue slide in Figure 4d shows that the microinjector tips penetrated only the mucosa layer of the rat colon. We observed that the submucosa and muscularis externa of microinjector administered tissue remained intact and exhibited the same morphology as the normal healthy rat colon control (Figure 4e). This result indicates that the microinjectors pose no concerns for colonic perforation and consequently are safe to use in the colon. Also, with regard to tissue damage, we note that due to the fact that the microinjector arms are ultrathin (approximately 5 μm), the incisions are thin and narrow as shown in Figure S5. Based on the histological results, we estimate that the tissue damage induced by microinjector insertion is tens of millions-fold smaller relative to the total area of the human gut. This minimal damage can recover quickly during mucosa regeneration (see Note S7 for a more detailed discussion). Furthermore, the animal model used in this study is a rat, which has a thinner colonic wall compared to that of a human. Thus, in light of future clinical translations, we believe the risk of perforation or mechanical damage to the intestinal epithelial barrier is minimal.

After demonstrating that the microinjectors could penetrate into the colon tissue *ex vivo*, we verified the operation of the microinjectors in live rats. For these experiments, we used 280-350 g male Wistar rats, which typically have a colon diameter of approximately 8 mm. We administered approximately 200 microinjectors through the rectum into the colon of these rats (Figure 5a) using a pneumatic microfluidic controller, which could eject a bolus of the microinjectors in saline using controlled pressure. We used a pressure of 14-16 psi with a medical-grade polycarbonate tubing with an internal diameter of 2.5 mm, to drive the bolus of microinjectors into the rat colon. We observed no adverse effect on the health of the animals during and even 48 h after the deployment of the microinjectors. Figure 5b,c shows μ-CT images of microinjectors still present and attached to the colon of rats 48 h after their intrarectal administration.

The microinjectors' function as an intraluminal drug injection device was tested using insulin as a model macromolecular drug in a live rat model, as has been done in the past.[21] We loaded insulin into the microinjector arms by soaking them in a concentrated insulin solution (see Materials and Methods).

First, we studied the *in vitro* release profile of insulin from the microinjectors over 4 h. We incubated 200 insulin-loaded microinjectors in saline at 37 °C and measured the released insulin in the solution over time. Based on these measurements, we estimate that each microinjector has the capacity to accommodate around 300 μIU of human insulin. Moreover, these measurements indicated that the microinjectors could steadily release insulin *in vitro* (Figure S6).

We then conducted *in vivo* insulin delivery experiments, in which 60 mIU of human insulin was administered per animal. Each experimental arm consisted of five rats and is described as follows: In the first arm, we delivered an intrarectal dose of 60 mIU of human insulin in 1 mL of saline (negative control). We delivered an intrarectal dose of 60 mIU of human insulin in the second arm, formulated with 200 microinjectors (experimental arm). We carried out the rectal administration for both groups using a pneumatic microfluidic controller. We administered an intravenous (IV) dose of 60 mIU of human insulin in the third group through a jugular vein catheter (positive control). We then drew blood from all the animals at t = 5 min, 30 min, 1, 2, 3, and 4 h post-administration of the insulin. We used a commercial enzyme-linked immunosorbent assay (ELISA) to determine human insulin concentration at various time points over the 4 h time window. The pharmacokinetic (PK) profile of human insulin in rat plasma over 4 h after administration is shown in Figure 5d. We measured peak plasma human insulin concentration administered by the microinjectors in the plasma of rats to be 9.6 μIU/mL at the 30 min time point. In contrast, the rats with intrarectally administered insulin solution without microinjectors (negative control arm) had only a minimal amount of human insulin in their plasma.

Furthermore, we measured the total exposure of insulin by calculating the area under the PK curves. The results are plotted in Figure 5e, where we see that the microinjectors provide similar total exposure of insulin in the bloodstream compared to the IV-dosed animals, although with a different PK profile. As expected, animals treated with IV insulin had a sharp increase in plasma level of insulin that then dropped precipitously. Animals treated with insulin-loaded microinjectors showed a slower increase but more sustained release, likely a function of absorption from the submucosal space into the systemic circulation.

We examined the insulin delivery efficiency of our microinjectors and compared that to other GI-tract-administered insulin delivery mechanisms. We made the comparison in terms of the maximum insulin plasma concentration as well as insulin dosage per body surface area (BSA) of the animals (details in Note S6). The microinjectors show a significantly higher insulin bioavailability in the rat model over other GI-tract-administered insulin vehicles. Specifically, we measured the highest human insulin plasma concentration of 65.3 pM in rats that received insulin-loaded microinjectors, with 0.063 mg/m^2 BSA initial dosage. We divided the highest plasma insulin concentration by the initial dosage to get a normalized insulin delivery coefficient of 1036.5 pM/mg·m^{-2} for microinjectors.

In comparison, the delivery coefficients in previously reported insulin delivery vehicles (studied in a rat GI tract) are as follows: (i) alginate/chitosan nanoparticles: 9.2 pM/mg·m^{-2}, (ii) HEMA nanogels: 9.5 pM/mg·m^{-2}, and (iii) hydrogel patches: 54.7 pM/mg·m^{-2}. [36-38] We attribute the high insulin delivery efficiency to the fact that the microinjector arms penetrated the GI mucosa, which greatly enhanced the macromolecular drug diffusion. Furthermore, we compared the insulin delivery efficiency of our microinjector with other GI-tract-based insulin injection devices studied in the pig model. For example, the SOMA device, which operates in the stomach, has a delivery coefficient of 111.1 pM/mg·m^{-2}. The LUMI device that works in the small intestine shows a delivery coefficient of 81.8 pM/mg·m^{-2}.[25,26] Though these GI tract insulin injection devices show a much better delivery efficiency compared to the delivery vehicles reported above, the microinjectors reported in this study outperform them by at least an order of magnitude. We believe that the use of many microinjectors in our study results in up to 600 microinjection sites compared to one [25] or tens of [26] injection sites created by other larger GI injection devices. The ability of the microinjectors to perform autonomous injection in small conduits like a rat GI tract also suggests the possibility of reaching narrower sites than the GI tract to perform localized drug delivery.

CONCLUSIONS

Oral administration of macromolecular drugs such as insulin for systemic delivery would dramatically improve patient outcomes and reduce costs by increasing compliance and decreasing complications and hospitalizations. However, enhancing the diffusion of these drug molecules across the GI epithelium is challenging. Here, we have introduced miniaturized microinjectors, which are small enough to be safely ingested and can significantly enhance the transportation of macromolecule drugs like insulin across the GI tract. Though the microinjectors are administered intrarectally in this work, we anticipate that an oral microinjector deployment vehicle will be incorporated in future work, such as a capsule with an enteric coating that can eject microinjectors into the GI tract. [25-26] Moreover, as the self-injecting device is independent of the encapsulated active molecule, the microinjector platform can be potentially formulated to deliver even fragile drugs such as peptides, antibodies, and RNA, which rarely have oral formulation. However, it remains to be seen how the design of the microinjectors can be scaled up for efficient delivery in large animal models, [25] which is essential for successful translation to the clinic. Though our method was found to be safe, in general, we envision that the use of transient and biodegradable materials to fabricate the microinjectors will further enhance the biocompatibility and safety of the proposed method of delivery.[39-40]

MATERIALS AND METHODS

Fabrication of the Microinjectors

We fabricated the microinjectors using planar microfabrication techniques on silicon wafers (Figure S1a). First, we deposited a sacrificial layer of copper (Cu, 300 nm) with underlying chromium (Cr) adhesion layer (20 nm) using thermal evaporation. The microinjector fabrication that followed on the top of the Cu layer consists of a combination

of photolithography, thermal evaporation of Cr and gold (Au), electrodeposition of nickel (Ni), Au, and chitosan, and spin-coating steps for the photoresist and wax. We fabricated microinjectors that actuate in one direction (unidirectional) or two directions (bidirectional) by incorporating one or two differentially stressed Cr/Au layers. For the bidirectional microinjector, each of the stress layer assemblies consists of three alternatively arranged microinjector tips. The details of the microinjector design are described in Note S1.

We fabricated the arms by creating a photolithographically defined pattern of six (for unidirectional) or three (for bidirectional) injection arms using the S1813 photoresist (Kayaku) on copper. We patterned the first stress layer assembly by evaporating 60 nm Cr/100 nm Au and liftoff. We then patterned the three alternate injection arms using a second photolithography step using the S1813 photoresist. This assembly consists of 15 nm Cr/100 nm Au/75 nm Cr /10 nm Au. After the stress layer deposition, we did photolithography using the SPR220 photoresist (Megaposit, Kayaku). We created the rigid panels on the differentially stressed multilayer assemblies by electroplating 3 μm of Ni and 0.3 μm of Au using commercial nickel sulfamate and gold sulfite solutions (Technic). [41] After photoresist stripping, we patterned a photoresist mold of SPR220 using photolithography on the microinjection tips. We filled the mold using chitosan (medium molecular weight, Sigma-Aldrich) using electrodeposition. We dissolved the photoresist mold (within 24 h) using acetone. We then patterned the paraffin wax (melting point 53-58 °C, Sigma-Aldrich) trigger layers on the hinges of the microinjectors using another step of photopatterning SPR220 photoresist on the hinges of the microinjectors. To ensure proper coverage of paraffin wax on the hinges of the microinjectors, we optimized the volume of wax dropped on the wafer and the spin-coating conditions. Further details of the fabrication optimization studies are in Note S2, Figure S2, and Table S2. After depositing the paraffin wax, we allowed the wax to sit for at least 2 h, and then we dissolved the photoresist. We then released the microinjectors from the wafer by dissolving the Cu sacrificial layer in a commercial basic cupric chloride solution (copper etchant BTP, Transene), which preserves the chitosan patch on the injection arms and the paraffin wax on the hinges. We thoroughly rinsed the injectors in DI water to remove any residual etchant.

In Vitro Gelatin Penetration Experiments

We prepared microbial transglutaminase (mTG) cross-linked gelatin hydrogels for the evaluation of the microinjector penetration as described previously.[35] Briefly, we dissolved 12.5% by weight gelatin powder (type A, porcine skin, Sigma-Aldrich) in phosphate-buffered saline (PBS) and sterile-filtered it through a 0.2 μm polystyrene membrane filter. We mixed the gelatin solution with 1 mL of sterile-filtered 10 U/g gelatin of mTG (Ajinomoto) prepared in PBS. We used Bloom 90-110 (low molecular weight, 20-25 kDa) and Bloom 300 (high molecular weight, 50-100 kDa) gelatin to prepare the 1 kPa (soft) and 35 kPa (stiff) hydrogels, respectively. We mixed 200 nm green, fluorescent polystyrene beads (Polysciences) with 350 μL of the gelatin-mTG solution to aid in visualization and added them to dishes with a 20 mm glass bottom (MatTek). We allowed the gel to cross-link for 8 h at 37 °C. After the cross-linking reaction, we heated the gelatin gels in PBS to 60 °C for 30 min to deactivate the mTG and stored them in PBS at 37 °C until subsequent use in the experiments.

To estimate the penetration of injector arms, we placed the microinjectors on the gelatin hydrogel surface under PBS, placed in an oven set at 40 °C. We observed that the wax trigger layer softened at this temperature and induced the folding of the injectors on the gelatin hydrogel surface. We imaged the microinjectors using a 10x objective on an A1 confocal microscope (Nikon) and estimated the injector tip penetration depth from the confocal z-stack using ImageJ. We created an orthogonal projection (side/xz view) of the confocal z-stack for each injector tip and measured the penetration depth from the hydrogel surface.

Ex Vivo Tissue Penetration Experiments

We used freshly excised rat colon and pig colon and stomach to carry out our *ex vivo* tissue penetration experiments with the microinjectors. We euthanized 300 g male Wistar rats (Charles River Laboratories) and removed the colon. We cleaned the colon and laid it flat to face up on the luminal side. We incubated the flat colon sections under saline and dropped microinjectors on the top of the tissue samples. We then placed the microinjectors/tissue assembly in an oven at 40 °C for 15-20 min. The microinjectors actuate at the increased temperature and penetrate their injection arms into the tissue. We performed similar experiments with pig colon and stomach. We procured the pig organs from freshly sacrificed animals from a butcher shop (Wagner Meats).

We characterized the penetration of microinjectors on *ex vivo* tissues using optical microscopy, scanning electron microscopy (JEOL), and microcomputed tomography imaging (RX Solutions). To image the tissue samples with microinjectors, we prepared the samples as follows: For optical microscopy and μ-CT, we used the fresh tissue, without any drying and fixing, to preserve the surface characteristics of the mucosa as much as possible. For SEM imaging, we collected the tissue samples with the penetrated microinjector arms. Then we used sodium cacodylate buffer to wash the tissue samples and fixed them in glutaraldehyde for an hour. We then washed the tissue in sodium cacodylate buffer and postfixed it in osmium tetroxide for 1 h on ice and in the dark. Afterward, we rinsed the tissue samples in DI water and performed tissue dehydration using a graded series of cold ethanol washes (50, 70, 90, and 100%) for 15 min each. We then successively soaked the samples at room temperature in the following solutions: anhydrous ethanol for 20 min two times, a mixture of 50% hexamethyldisilazane (HMDS), and 50% anhydrous ethanol for 30 min, and finally pure HMDS for 30 minutes. We air-dried the samples before putting them in the SEM instrument.

We also performed a histological study to characterize the penetration of the microinjector tips. We positioned the *ex vivo* rat colon tissue sample with actuated microinjectors in a cryostat mold and embedded the tissue sample using an OCT compound (Tissue-Tek, Sakura Finetek USA). Then we transferred the embedded tissue samples into a −80 °C freezer for at least 30 min to freeze the samples properly. We removed the frozen samples from the mold and mounted the sample on a cryostat microtome (Tanner Scientific, TN60). We trimmed the sample until the desired microinjector penetration location was observed. We then switched the cryostat to the sectioning mode with a slicing thickness from 10 to 30 μm and cut the sample slices. Afterward, we flattened and loaded the sample slices onto glass slides. We

imaged the freshly sectioned slides with a microscope (ZEISS, Axio Vert A1). The sample slides were stored in a −80 °C freezer before fixation and H&E staining. The H&E-stained sample slides were imaged using a microscope (ZEISS, Axio Vert A1).

In Vitro Measurements of Insulin Release from Microinjectors

To prepare the insulin-loaded microinjectors, we released around 100 microinjectors from the silicon wafer by dissolving the Cu sacrificial layer and rinsing at least six times to remove the Cu etchant and obtain a clear solution of microinjectors in DI water. We then replaced the DI water with 5 mg/mL of human insulin saline solution, in which we soaked the microinjectors for 36 h at room temperature (around 23 °C). After that, we washed the microinjectors with DI water at least six times to remove the excess insulin.

We conducted the *in vitro* human insulin release experiments by immersing around 100 microinjectors in 10 mL of saline at 37 °C. At each desired time point, we withdrew 100 μL from the solution and replaced it with 100 μL of fresh saline to maintain a proper sink condition. We then measured the concentrations of human insulin in the samples at various time points using a commercial ELISA kit (ALPCO, 80-INSHU-E01.1) and a spectrophotometer (Molecular Devices, SpectraMax i3). We repeated the experiment three times and plotted the cumulative concentrations in Figure S6.

In Vivo Insulin Delivery Experiments Using Microinjectors

We prepared the human insulin-loaded microinjectors for *in vivo* animal experiments using the same method described in the *in vitro* experiment section above. We used 200 (±2%) microinjectors for each animal. We performed the *in vivo* experiments on male Wistar rats with a jugular vein catheter weighing approximately 300 g (Charles River Laboratories). The experiments followed the Johns Hopkins University Animal Care and Use Committee protocol number RA19M207. We fasted the rats for 1 day before the experiments for an empty colon. We mildly anesthetized the rats using isoflurane and oxygen while intrarectally administering the microinjectors. We stored the human insulin-loaded microinjectors in 2 mL vials. To deliver the microinjectors, we attached a medical-grade polytetrafluoroethylene tube with a 2.5 mm inner diameter (Zeus) to a computer-controlled pneumatic delivery system (Fluigent, MFCS-100 1C). We inserted it 3-4 cm inside the colon of the animal. We ejected the microinjectors with a small amount of DI water at 14-16 psi pressure (Figure 5a). We returned the rats to the cage after microinjector administration.

We drew a 100 μL blood sample *via* the jugular vein cannula for bioanalysis at the predefined time points. We mixed the blood samples with 20 IU heparin and then centrifuged them at 3000 rcf for 10 min to separate the plasma. We stored the resulting plasma at −80 °C until the insulin assay measurements.

Assay for the Detection of Human Insulin in Rats

We used ELISA to conduct the insulin concentration measurements following the manufacturer-directed assay procedure. Briefly, to determine insulin concentration in rat plasma, we used an ultrasensitive human insulin-specific ELISA kit (ALPCO, 80-INSHUU-E01.1), having a sensitivity of 0.135 μIU/mL and a dynamic range of 0.15-20 μIU/mL,

which is insensitive to rat intrinsic insulin. To determine insulin concentrations in saline in our *in vitro* release experiments, we used an ELISA kit (ALPCO, 80-INSHU-E01.1) with a sensitivity of 0.399 μIU/mL and a dynamic range of 3.0-200 μIU/mL. We used a microplate shaker (800 rpm) to carry out the reaction of the rat plasma samples and the detection antibody in a 96 well-plate, which is precoated with a monoclonal antibody specific to human insulin. We duplicated each plasma sample during the measurement for each time point and each animal. We used rat plasma collected before the insulin administration as the control and used the manufacturer-provided standard solutions during the analysis. After the reaction with the antibodies, we washed the wells thoroughly with a buffer. We then used colorimetric detection to measure the absorbance of each well at 450 nm wavelength with a spectrophotometer (Molecular Devices, SpectraMax i3). We compared the absorbances with a previously obtained standard curve of human insulin (Figure S7), acquired using the manufacturer-provided standard solutions. We plotted the extracted insulin concentrations as a function of the time of sample collection (Figure 5d) and the area under the curve (Figure 5e) for the different experiments. Please see Note S5 for further details about the insulin dose determination and assay validation procedure (Figure S8).

Supplementary Material

Refer to Web version on PubMed Central for supplementary material.

ACKNOWLEDGMENTS

We acknowledge the support from Department of Pathology, Johns Hopkins Hospital for help with H&E tissue staining. Research reported in this publication was supported by the National Institute of Biomedical Imaging and Bioengineering of the National Institutes of Health under Award Number R01EB017742. The content is solely the responsibility of the authors and does not necessarily represent the official views of the National Institutes of Health.

REFERENCES

[1]. Banting FG, Best CH, Collip JB, Campbell WR, Fletcher AA, Pancreatic Extracts in the Treatment of Diabetes Mellitus. Can. Med. Assoc. J 1922, 12, 141. [PubMed: 20314060]

[2]. Lin X, Xu Y, Pan X, Xu J, Ding Y, Sun X, Song X, Ren Y, Shan P-F, Global, Regional, and National Burden and Trend of Diabetes in 195 Countries and Territories: An Analysis From 1990 to 2025. Sci. Rep 2020, 10, 14790. [PubMed: 32901098]

[3]. Anselmo AC, Gokarn Y, Mitragotri S, Non-Invasive Delivery Strategies for Biologics. Nat. Rev. Drug Discov 2019, 18, 19. [PubMed: 30498202]

[4]. Prausnitz MR, Microneedles for Transdermal Drug Delivery. Adv. Drug Deliv. Rev 2004, 56, 581. [PubMed: 15019747]

[5]. Martanto W, Davis SP, Holiday NR, Wang J, Gill HS, Prausnitz MR, Transdermal Delivery of Insulin Using Microneedles In Vivo. Pharm. Res 2004, 21, 947. [PubMed: 15212158]

[6]. McAllister DV, Wang PM, Davis SP, Park J-H, Canatella PJ, Allen MG, Prausnitz MR, Microfabricated Needles for Transdermal Delivery of Macromolecules and Nanoparticles: Fabrication Methods and Transport Studies. Proc. Natl. Acad. Sci. U. S. A 2003, 100, 13755. [PubMed: 14623977]

[7]. Prausnitz MR, Langer R, Transdermal Drug Delivery. Nat. Biotechnol 2008, 26, 1261. [PubMed: 18997767]

[8]. Zhou C-P, Liu Y-L, Wang H-L, Zhang P-X, Zhang J-L, Transdermal Delivery of Insulin Using Microneedle Rollers In Vivo. Int. J. Pharm 2010, 392, 127. [PubMed: 20347024]

[9]. Zhao J, Xu G, Yao X, Zhou H, Lyu B, Pei S, Wen P, Microneedle-Based Insulin Transdermal Delivery System: Current Status and Translation Challenges. Drug Deliv. Transl. Res 2021; DOI: 10.1007/s13346-021-01077-3

[10]. Zhang N, Zhou X, Liu L, Zhao L, Xie H, Yang Z, Dissolving Polymer Microneedles for Transdermal Delivery of Insulin. Front. Pharmacol 2021, 12, 719905. [PubMed: 34630098]

[11]. Fonte P, Araújo F, Reis S, Sarmento B, Oral Insulin Delivery: How Far Are We? J. Diabetes Sci. Technol 2013, 7, 520. [PubMed: 23567010]

[12]. Caffarel-Salvador E, Abramson A, Langer R, Traverso G, Oral Delivery of Biologics Using Drug-Device Combinations. Curr. Opin. Pharmacol 2017, 36, 8. [PubMed: 28779684]

[13]. Morishita M, Peppas NA, Is the Oral Route Possible for Peptide and Protein Drug Delivery? Drug Discov. Today 2006, 11, 905. [PubMed: 16997140]

[14]. Saffran M, Kumar GS, Savariar C, Burnham JC, Williams F, Neckers DC, A New Approach to the Oral Administration of Insulin and Other Peptide Drugs. Science 1986, 233, 1081. [PubMed: 3526553]

[15]. Kimura T, Sato K, Sugimoto K, Tao R, Murakami T, Kurosaki Y, Nakayama T, Oral Administration of Insulin As Poly (vinyl alcohol)-Gel Spheres in Diabetic Rats. Biol. Pharm. Bull 1996, 19, 897. [PubMed: 8799497]

[16]. Damgé C, Vranckx H, Balschmidt P, Couvreur P, Poly (alkyl cyanoacrylate) Nanospheres for Oral Administration of Insulin. J. Pharm. Sci 1997, 86, 1403. [PubMed: 9423155]

[17]. Goldberg M, Gomez-Orellana I, Challenges for the Oral Delivery of Macromolecules. Nat. Rev. Drug Discov 2003, 2, 289. [PubMed: 12669028]

[18]. Brown TD, Whitehead KA, Mitragotri S, Materials for Oral Delivery of Proteins and Peptides. Nat. Rev. Mater 2020, 5, 127.

[19]. Tyagi P, Pechenov S, Anand Subramony J, Oral Peptide Delivery: Translational Challenges Due to Physiological Effects. J. Control. Release 2018, 287, 167. [PubMed: 30145135]

[20]. Aungst BJ, Intestinal Permeation Enhancers. J. Pharm. Sci 2000, 89, 429. [PubMed: 10737905]

[21]. Maher S, Mrsny RJ, Brayden DJ, Intestinal Permeation Enhancers for Oral Peptide Delivery. Adv. Drug Deliv. Rev 2016, 106, 277. [PubMed: 27320643]

[22]. Salama NN, Eddington ND, Fasano A, Tight Junction Modulation and Its Relationship to Drug Delivery. Adv. Drug Deliv. Rev 2006, 58, 15. [PubMed: 16517003]

[23]. Moroz E, Matoori S, Leroux J-C, Oral Delivery of Macromolecular Drugs: Where We Are After Almost 100 Years of Attempts. Adv. Drug Deliv. Rev 2016, 101, 108. [PubMed: 26826437]

[24]. Doak BC, Over B, Giordanetto F, Kihlberg J, Oral Druggable Space Beyond the Rule of 5: Insights From Drugs and Clinical Candidates. Chem. Biol 2014, 21, 1115. [PubMed: 25237858]

[25]. Abramson A, Caffarel-Salvador E, Khang M, Dellal D, Silverstein D, Gao Y, Frederiksen MR, Vegge A, Hubálek F, Water JJ, Friderichsen AV, Fels J, Kirk RK, Cleveland C, Collins J, Tamang S, Hayward A, Landh T, Buckley ST, Roxhed N, Rahbek U, Langer R, Traverso G, An Ingestible Self-Orienting System for Oral Delivery of Macromolecules. Science 2019, 363, 611. [PubMed: 30733413]

[26]. Abramson A, Caffarel-Salvador E, Soares V, Minahan D, Tian RY, Lu X, Dellal D, Gao Y, Kim S, Wainer J, Collins J, Tamang S, Hayward A, Yoshitake T, Lee H-C, Fujimoto J, Fels J, Frederiksen MR, Rahbek U, Roxhed N, Langer R, Traverso G, A Luminal Unfolding Microneedle Injector for Oral Delivery of Macromolecules. Nat. Med 2019, 25, 1512. [PubMed: 31591601]

[27]. Aran K, Chooljian M, Paredes J, Rafi M, Lee K, Kim AY, An J, Yau JF, Chum H, Conboy I, Murthy N, Liepmann D, An Oral Microjet Vaccination System Elicits Antibody Production in Rabbits. Sci. Transl. Med 2017, 9, eaaf6413 . [PubMed: 28275153]

[28]. Dhalla AK, Al-Shamsie Z, Beraki S, Dasari A, Fung LC, Fusaro L, Garapaty A, Gutierrez B, Gratta D, Hashim M, Horlen K, Karamchedu P, Korupolu R, Liang E, Ong C, Owyang Z, Salgotra V, Sharma S, Syed B, Syed M, Vo AT, Abdul-Wahab R, Wasi A, Yamaguchi A, Yen S, Imran M, A Robotic Pill for Oral Delivery of Biotherapeutics: Safety, Tolerability, and Performance in Healthy Subjects. Drug Deliv. Transl. Res 2022, 12, 294. [PubMed: 33604838]

[29]. Nikolaus S, Schreiber S, Diagnostics of Inflammatory Bowel Disease. Gastroenterology 2007, 133, 1670. [PubMed: 17983810]

[30]. Bassik N, Stern GM, Gracias DH, Microassembly Based on Hands Free Origami With Bidirectional Curvature. Appl. Phys. Lett 2009, 95, 91901. [PubMed: 19787072]

[31]. Bassik N, Brafman A, Zarafshar AM, Jamal M, Luvsanjav D, Selaru FM, Gracias DH, Enzymatically Triggered Actuation of Miniaturized Tools. J. Am. Chem. Soc 2010, 132, 16314. [PubMed: 20849106]

[32]. Gultepe E, Randhawa JS, Kadam S, Yamanaka S, Selaru FM, Shin EJ, Kalloo AN, Gracias DH, Biopsy with Thermally-Responsive Untethered Microtools. Adv. Mater 2013, 25, 514. [PubMed: 23047708]

[33]. Ghosh A, Li L, Xu L, Dash RP, Gupta N, Lam J, Jin Q, Akshintala V, Pahapale G, Liu W, Sarkar A, Rais R, Gracias DH, Selaru FM, Gastrointestinal-Resident, Shape-Changing Microdevices Extend Drug Release In Vivo. Sci. Adv 2020, 6. eabb4133. [PubMed: 33115736]

[34]. Stewart DC, Berrie D, Li J, Liu X, Rickerson C, Mkoji D, Iqbal A, Tan S, Doty AL, Glover SC, Simmons CS, Quantitative Assessment of Intestinal Stiffness and Associations with Fibrosis in Human Inflammatory Bowel Disease. PLoS One 2018, 13, e0200377. [PubMed: 29995938]

[35]. Pahapale GJ, Gao S, Romer LH, Gracias DH, Hierarchically Curved Gelatin for 3D Biomimetic Cell Culture. ACS Appl. Bio Mater 2019, 2, 6004.

[36]. Sarmento B, Ribeiro A, Veiga F, Sampaio P, Neufeld R, Ferreira D, Alginate/Chitosan Nanoparticles Are Effective for Oral Insulin Delivery. Pharm. Res 2007, 24, 2198. [PubMed: 17577641]

[37]. Whitehead K, Shen Z, Mitragotri S, Oral Delivery of Macromolecules Using Intestinal Patches: Applications for Insulin Delivery. J. Control. Release 2004, 98, 37. [PubMed: 15245887]

[38]. Wang X, Cheng D, Liu L, Li X, Development of Poly (hydroxyethyl methacrylate) Nanogel for Effective Oral Insulin Delivery. Pharm. Dev. Technol 2018, 23, 351. [PubMed: 28655281]

[39]. Yin L, Cheng H, Mao S, Haasch R, Liu Y, Xie X, Hwang S, Jain H, Kang S, Su Y, Li R, Huang Y, Rogers JA, Dissolvable Metals for Transient Electronics. Adv. Funct. Mater 2014, 24, 644.

[40]. Yun Y, Dong Z, Lee N, Liu Y, Xue D, Guo X, Kuhlmann J, Doepke A, Brian Halsall H, Heineman W, Sundaramurthy S, Schulz MJ, Yin Z, Shanov V, Hurd D, Nagy P, Li W, Fox C, Revolutionizing Biodegradable Metals. Mater. Today 2009, 12, 22.

[41]. Leong TG, Randall CL, Benson BR, Bassik N, Stern GM, Gracias DH, Tetherless Thermobiochemically Actuated Microgrippers. Proc. Natl. Acad. Sci. U. S. A 2009, 106, 703. [PubMed: 19139411]

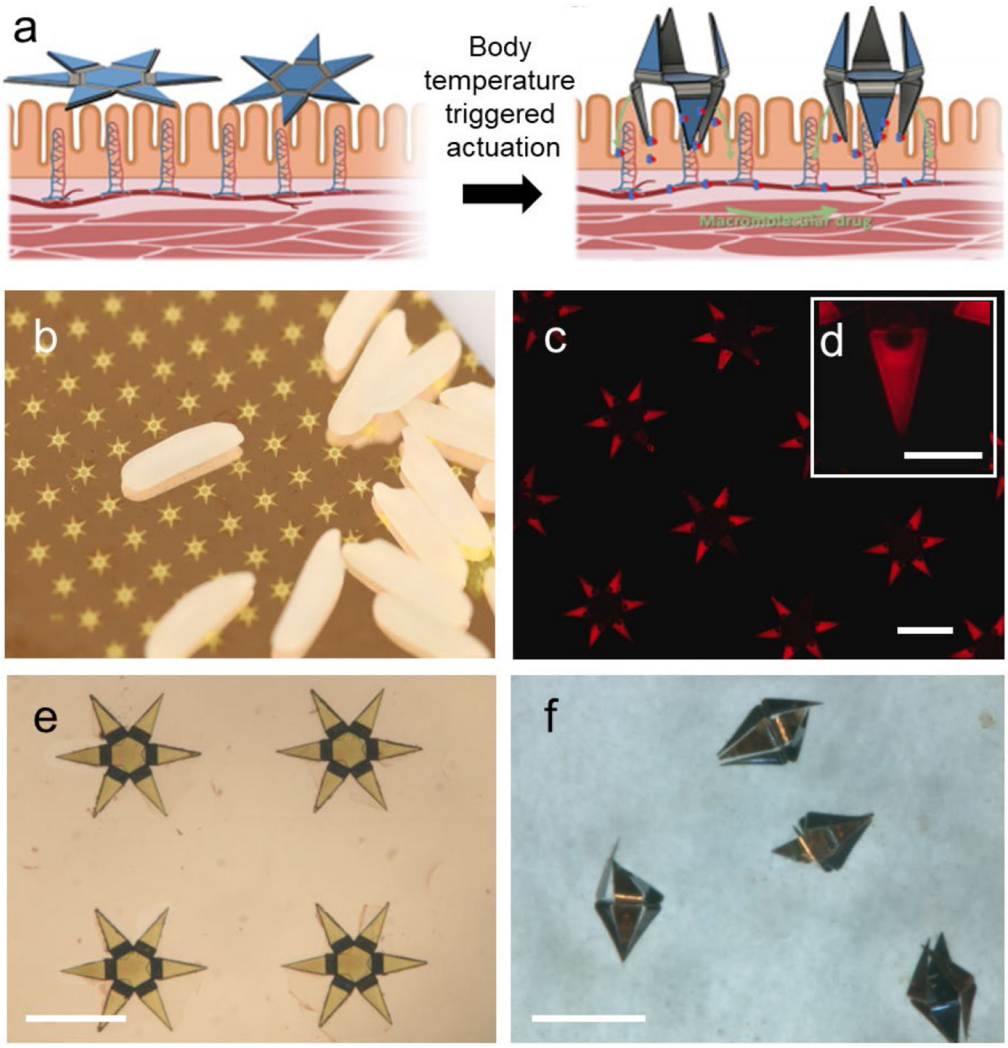

Figure 1. Design, fabrication, and operation of autonomous microinjectors.

(a) Conceptual illustration showing autonomous actuation of two microinjectors with their injection arms penetrating the mucosa as the injectors equilibrate to physiological temperature, while the macromolecular drugs are transported across the mucosal epithelium. Elements created with BioRender.com with publication license. (b) Photo of microinjector arrays fabricated on a silicon wafer near rice grains, illustrating the small size of the microinjectors and parallel wafer-scale fabrication. (c) Fluorescence image of an array of as-fabricated microinjectors loaded with fluorescent rhodamine within chitosan gel to aid visualization of the drug patches on the injection tips. The scale bar is 1 mm. (d) The inset shows a zoomed fluorescence image of a single injection tip loaded with fluorescent rhodamine within the chitosan gel patches. The scale bar is 200 μm. (e-f) Optical microscopy images of microinjectors, (e) as-fabricated on a silicon wafer, and (f) bidirectionally folded post actuation in response to a physiological temperature. The scale bars are 1 mm.

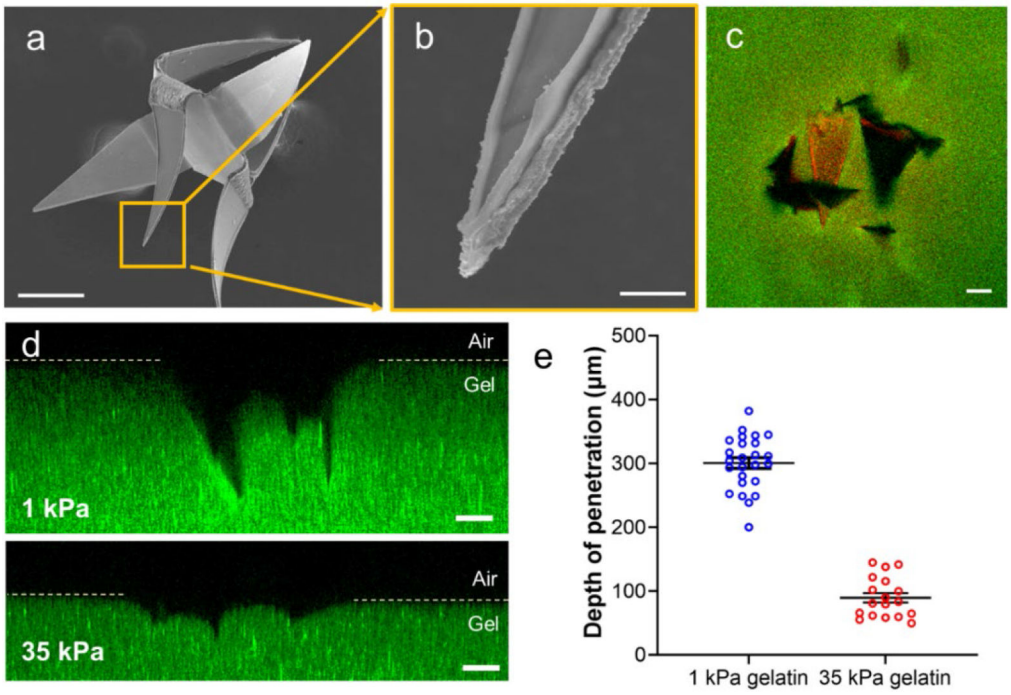

Figure 2: Evaluation of the penetration of the microinjector arms into tissue-mimicking gelatin hydrogels.

(a) Scanning electron microscope (SEM) image of a bidirectional microinjector after actuation, illustrating that the injector arms fold in opposite directions. The scale bar is 200 μm. (b) Magnified SEM image of a microinjector showing the insulin-loaded chitosan patch on the tip. The scale bar is 10 μm. (c) Confocal image showing the top view of the microinjector (the chitosan gel on microinjector tips is loaded with rhodamine dye for visualization) penetrating a 1 kPa gelatin hydrogel (loaded with 200 nm diameter fluorescent polystyrene beads for visualization). The scale bar is 100 μm. (d) Cross-sectional confocal fluorescence microscopy image (side view) of the microinjector tips penetrating a 1 kPa (top) and a 35 kPa (bottom) gelatin hydrogel. The images show that the microinjection tips penetrate significantly deeper into the soft 1 kPa gelatin. The scale bars are 100 μm. (e) Plot depicting the depth of penetration of the microinjector tips into the gelatin hydrogels of two different stiffnesses, 1 kPa (blue) and 35 kPa (red). Data presented were measured for each of the three penetrated microinjector tips from at least 4 samples, and the plot shows the mean and standard error of the mean.

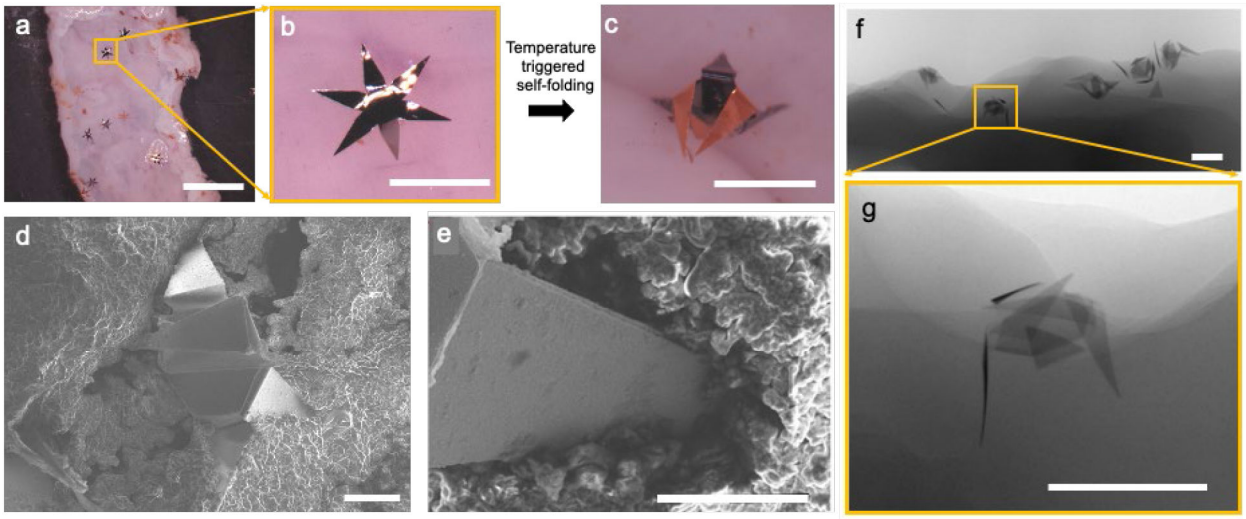

Figure 3: Autonomous operation of the microinjectors on *ex vivo* rat colon.

(a) Optical image showing microinjectors before actuation on freshly excised rat colon tissue *ex vivo.* The scale bar is 5 mm. (b-c) Zoomed images of a microinjector, (b) before, and (c) after autonomous actuation at physiological temperature. The scale bars are 1 mm. (d) SEM image of a microinjector attached to the rat colon tissue. The scale bar is 200 μm. (e) SEM image showing the penetration of an injection tip into the colon tissue. The scale bar is 100 μm. (f) μ-CT image of an *ex vivo* rat colon with microinjectors attached to it. The scale bar is 1 mm. (g) Zoomed in μ-CT image of the microinjector marked in panel f, showing the depth of penetration into the tissue. The scale bar is 1 mm.

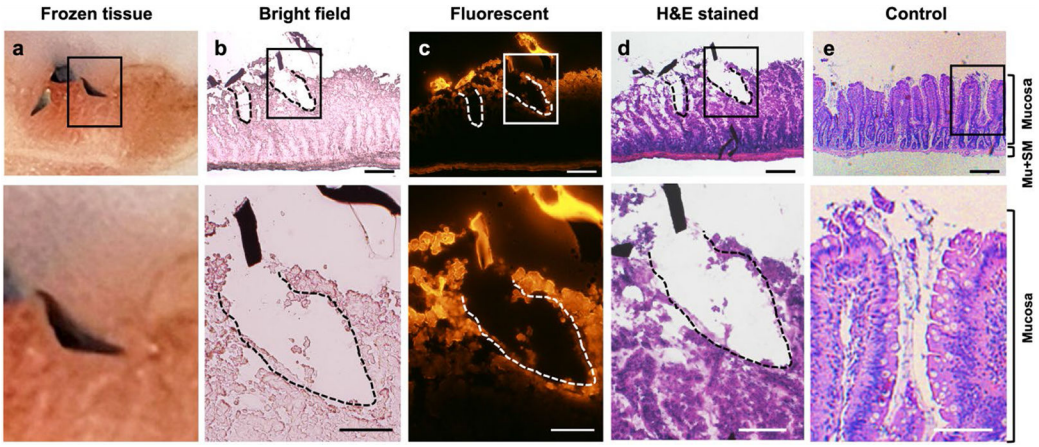

Figure 4: Rat colon histology after microinjector actuation.

The top panel shows microinjector tips inserted in the tissue. The bottom panel show the magnified view of corresponding upper panel. The scale bars in top panel are 200 μm, and the scale bars in bottom panel are 100 μm. (a) Photo showing the cross-section of rat tissue with a microinjector penetrated during the frozen sectioning process on microtome. The colon tissue is embedded and frozen in Optimal Cutting Temperature compound (OCT). (b) Bright field microscopic image of freshly sectioned colon tissue slide at the injection site. Two incisions created by the microinjector tips and the sliced debris of microinjector arm were observed. The incision depth is 259 μm (left), and 332 μm (right). (c) Fluorescent microscopic image of colon tissue slide at the injection site. Microinjector tips were loaded with fluorescent dye Rhodamine 6G which was released at the injection site, indicated by the staining of the nearby tissue (red fluorescence). (d) Microscopic image of hematoxylin and eosin (H&E)-stained colon tissue at the insert site of microinjector. (e) Microscopic image of H&E-stained control colon. Mu, muscularis externa; SM, submucosa.

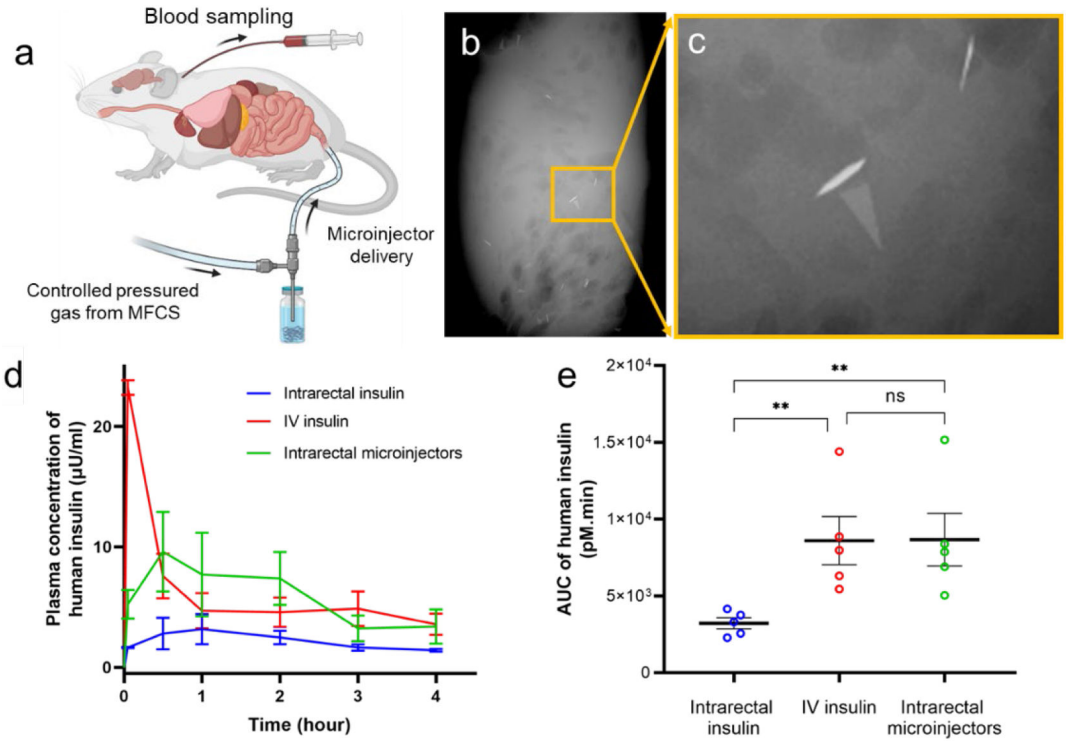

Figure 5: Enteral delivery of human insulin using microinjectors in live rats.

(a) Schematic of the *in vivo* experiments, which involve the intrarectal administration of human insulin formulated microinjectors. The microinjectors were delivered at a controlled air pressure using a microfluidic controller. Elements of the schematic are created with BioRender.com with a publication license. (b-c) μ-CT image of the excised colon, 48 hours post rectal administration in rats, showing the presence of microinjectors attached to the colon (d) Pharmacokinetic (PK) profile showing the concentration (mean and standard error of the mean) of human insulin measured in rat plasma after administration over four hours. In these studies, the insulin was injected intravenously (red, positive control), intrarectally using microinjectors (green), and intrarectally (blue, negative control) using the microfluidic controller. Each experimental arm was conducted for five different male rats. (e) Plot showing the comparison of the area under the PK curves in panel d. The plot shows that the microinjectors can lead to similar levels of total exposure to insulin as compared to IV insulin. The plot shows the mean and standard error of the mean (N=5). ** means $p < 0.01$